Metabolic Imaging of Cerebral Gliomas: Spatial Correlation of Changes in *O*-(2-^{18}F-Fluoroethyl)-L-Tyrosine PET and Proton Magnetic Resonance Spectroscopic Imaging

Andreas Stadlbauer[1,2], Olaf Prante[3], Christopher Nimsky[1], Erich Salomonowitz[2], Michael Buchfelder[1], Torsten Kuwert[3], Rainer Linke[3], and Oliver Ganslandt[1]

[1]Department of Neurosurgery, University of Erlangen-Nuremberg, Erlangen, Germany; [2]MR Physics Group, Department of Radiology, Landesklinikum St. Poelten, St. Poelten, Austria; and [3]Clinic of Nuclear Medicine, University of Erlangen-Nuremberg, Erlangen, Germany

The aim of this study was to determine the spatial correlation of *O*-(2-^{18}F-fluoroethyl)-L-tyrosine (^{18}F-FET) uptake and the concentrations of choline (Cho), creatine (Cr), and total *N*-acetylaspartate (tNAA) determined with proton magnetic resonance spectroscopic imaging (^{1}H MRSI) in cerebral gliomas for the multimodal evaluation of metabolic changes. **Methods:** ^{18}F-FET PET and 2-dimensional ^{1}H MRSI were performed in 15 patients with cerebral gliomas of World Health Organization (WHO) grades II–IV. PET and ^{1}H MRSI datasets were coregistered by use of mutual information. On the basis of their levels of ^{18}F-FET uptake, 4 different areas in a tumor (maximum, strong, moderate, and low ^{18}F-FET uptake) were defined on PET slices as being congruent with the volume of interest in the ^{1}H MRSI experiment. ^{18}F-FET uptake in lesions was evaluated as tumor-to-brain ratios. Metabolite concentrations for Cho, Cr, and tNAA and Cho/tNAA ratios were computed for these 4 areas in the tumor and for the contralateral normal brain. **Results:** In the area with maximum ^{18}F-FET uptake, the concentration of tNAA ($R = -0.588$) and the Cho/tNAA ratio ($R = 0.945$) correlated significantly with ^{18}F-FET uptake. In the areas with strong and moderate ^{18}F-FET uptake, only the Cho/tNAA ratios ($R = 0.811$ and $R = 0.531$, respectively) were significantly associated with amino acid transport. At low ^{18}F-FET uptake, analysis of the correlations of amino acid uptake and metabolite concentrations yielded a significant result only for the concentration of Cr ($R = 0.626$). No correlation was found for metabolite concentrations determined with ^{1}H MRSI and ^{18}F-FET uptake in normal brain tissue. Maximum ^{18}F-FET uptake and the tNAA concentration were significantly different between gliomas of WHO grades II and IV, with *P* values of 0.032 and 0.016, respectively. **Conclusion:** High ^{18}F-FET uptake, which is indicative of tumor cell infiltration, associates with neuronal cell loss (tNAA) and changes in ratios between parameters representing membrane proliferation and those of neuronal loss (Cho/tNAA ratio), which can be measured by ^{1}H MRSI. The significant correlation coefficients detected for Cr in regions with low ^{18}F-FET uptake suggests an association between the mechanism governing amino acid transport and energy metabolism in areas that are infiltrated by tumor cells to a lesser extent. These findings motivate further research directed at investigating the potential of ^{1}H MRSI to define tumor boundaries in a manner analogous to that of amino acid PET.

Key Words: metabolic imaging; brain tumor; magnetic resonance spectroscopy; PET; tyrosine

J Nucl Med 2008; 49:721–729
DOI: 10.2967/jnumed.107.049213

In clinical practice, CT and MRI are the methods of choice for the detection and diagnosis of brain tumors. However, the main limiting factor of these imaging methods is the lack of metabolic information on pathologic changes, which is in fact attributable to their imaging principles: assessment of differences in absorption coefficients in the case of CT and variations in density and derived parameters (e.g., relaxation times) of water and fat protons in the case of MRI. Hence, it is often difficult to assess the entire extent of the pathology in brain tumors by CT or MRI, even after the application of contrast medium.

PET is currently the most powerful method of molecular imaging. PET with ^{18}F-FDG is well accepted and widely used in the grading of brain tumors. However, the low tumor-to-background contrast, attributable to the high glucose uptake of the normal cortex, makes the delineation of the extent of these lesions difficult. Furthermore, the uptake of ^{18}F-FDG by tumor cells is not specific for neoplastic tissue; it has been observed in infections or inflammations as well (*1–3*). To overcome these limitations, radiolabeled amino acids such as [methyl-^{11}C]-L-methionine and amino acid analogs such as *O*-(2-^{18}F-fluoroethyl)-L-tyrosine (^{18}F-FET) have been developed. It has been demonstrated that

Received Nov. 17, 2007; revision accepted Jan. 30, 2008.
For correspondence or reprints contact: Andreas Stadlbauer, Department of Neurosurgery, University of Erlangen-Nuremberg, Schwabachanlage 6, D-91054 Erlangen, Germany.
E-mail: andi@nmr.at

amino acids appear to be more specific tumor imaging agents because amino acid transport and protein metabolism are significantly upregulated in brain tumors in comparison with normal brain tissue and inflammatory sites (*4–6*). ^{18}F-FET is not incorporated into proteins, and the underlying mechanisms of ^{18}F-FET uptake in vivo are still not fully clarified and are still under discussion (*7*).

Proton magnetic resonance spectroscopic imaging (^{1}H MRSI) is another method of metabolic imaging that allows for investigation of the spatial distribution of metabolites in normal tissue and pathologic changes. Although in vivo ^{1}H MRSI is not able to quantify tumor-specific metabolites, it can detect specific patterns in the changes in metabolite concentrations compared with those in normal brain tissue. Gliomas are characterized by an increased level of choline-containing compounds (Cho) and a reduction in the signal intensity of *N*-acetylaspartate (NAA) (*8*). These changes correlate well with tumor cell infiltration in solid tumors and correlate somewhat in the infiltration zone of gliomas (*9*). The ^{1}H MRSI signal of Cho is composed of choline, phosphocholine, phosphatidylcholine, and glycerophosphocholine. Cho is a marker for increased cell membrane proliferation or higher cellular density (*10*). NAA is regarded as a neuronal marker mainly contained within neurons, where it is involved as an osmolyte in the fluid balance of the brain and in the synthesis of, for example, myelin and *N*-acetylaspartylglutamate (NAAG) (*11*). Because NAA is quite difficult to resolve from NAAG with in vivo ^{1}H MRSI, it is common practice to determine the concentrations of NAA and NAAG as total NAA (tNAA). The creatine (Cr) peak originates from both creatine and phosphocreatine, which play a role in tissue energy metabolism (*12*).

Both metabolic imaging techniques provide insight into metabolic changes related to pathologic processes. The purpose of this study was to correlate the metabolic changes in gliomas investigated by these 2 different metabolic imaging methods, that is, ^{18}F-FET PET and ^{1}H MRSI, to provide sophisticated information about pathologic changes in metabolism for areas with variable extents of tumor infiltration. ^{18}F-FET PET and ^{1}H MRSI datasets were coregistered with an anatomic 3-dimensional (3D) MRI dataset, allowing for the direct correlation of changes in amino acid uptake and changes in membrane, energy, and neuronal metabolism.

MATERIALS AND METHODS

Patient Population

Fifteen patients (9 men; mean ± SD age, 45 ± 16 y; age range, 23–78 y) with cerebral gliomas were included in this study. Four patients had gliomas of World Health Organization (WHO) grade II, 5 patients had gliomas of WHO grade III, 1 patient had gliomatosis cerebri, and 5 patients had glioblastoma multiforme (GBM) of WHO grade IV (Table 1). All lesions were confirmed histopathologically with tissue samples obtained by a frameless stereotactic procedure after preoperative diagnosis with conventional MRI, ^{1}H MRSI, and ^{18}F-FET PET. For cases with congruence in the areas with maximum ^{18}F-FET uptake and maximum changes in Cho/tNAA ratios of more than 50%, biopsies were obtained from the area of overlap. For cases with an overlap of less than 50%, biopsies were obtained from the area with maximum ^{18}F-FET uptake.

The datasets of the ^{1}H MRSI and PET experiments were acquired within 2 wk and retrospectively correlated. PET was performed as part of the routine preoperative diagnostic workup of gliomas at our institution. The ethics committee of the Department of Neurosurgery, Erlangen, gave its approval for the MR experiments.

TABLE 1
Clinical Data for 15 Patients

Patient	Age (y)	Sex	Histologic diagnosis	Location	Overlap of maxima*
1	51	F	Astrocytoma of WHO grade III	R, frontotemporal	2
2	29	M	Astrocytoma of WHO grade II	L, postcentral	2
3	37	F	Oligoastrocytoma of WHO grade III	R, frontal	2
4	34	M	GBM of WHO grade IV	L, temporoparietal	2
5	39	F	GBM of WHO grade IV	L, frontal	2
6	57	F	Astrocytoma of WHO grade III	L, frontal	1
7	54	M	Astrocytoma of WHO grade III	L, frontal	1
8	38	M	Astrocytoma of WHO grade II	L, frontoparietal	2
9	23	F	Oligoastrocytoma of WHO grade II	R, occipital	2
10	24	F	Astrocytoma of WHO grade III	L, frontal	2
11	78	M	Gliomatosis cerebri	R, temporal	1
12	43	M	GBM of WHO grade IV	R, temporal	1
13	66	M	GBM of WHO grade IV	L, temporal	2
14	59	M	GBM of WHO grade IV	R, frontal	2
15	43	M	Oligoastrocytoma of WHO grade II	R, parietal	2

*Overlap of maxima = estimation of overlap between area with maximum ^{18}F-FET uptake and area with maximum changes in corresponding Cho/tNAA ratio maps: 2 = 100%–50% overlap; 1 = <50% but more than no overlap; 0 = no overlap.
R = right hemisphere; L = left hemisphere.

MRI and ^{1}H MRSI

The MR examinations were performed on a 1.5-T clinical whole-body scanner (Sonata; Siemens) equipped with the standard head coil. The conventional MRI protocol consisted of an axial turbo spin-echo sequence (T2 weighted; 5-mm section thickness; repetition time [TR]/echo time [TE] = 5,600–6,490/98 ms), an axial fluid-attenuated inversion recovery sequence (5-mm section thickness; TR/TE = 10,000/103 ms), and a pre- and postgadolinium contrast-enhanced anatomic 3D magnetization-prepared rapid acquisition gradient-echo (MPRAGE) sequence (1-mm isotropic voxels; 160 slices; TR/TE = 2,020/4.38 ms).

An axial spin-echo (SE) sequence (T1 weighted; TR/TE = 500/15 ms; matrix size, 256 × 256; field of view, 16 × 16 cm; 20 slices with no gap; slice thickness, 2 mm) was used for planning the ^{1}H MRSI experiment and for the coregistration of spectroscopic data with anatomic MRI data (*13*). For preselection of the volume of interest for the ^{1}H MRSI experiment, a point-resolved spectroscopy (PRESS) sequence scheme was used. The volume of interest was aligned parallel to the axial T1-weighted SE slices and positioned to exclude lipids of the skull and subcutaneous fat. Water suppression was achieved with 3 chemical shift–selective pulses before the PRESS excitation. The ^{1}H MRSI parameters were as follows: TR/TE = 1,600/135 ms; 24 × 24 circular phase encoding scheme across a field of view of 16 × 16 cm; slice thickness, 1 cm; 50% Hamming filter; and 2 excitations. The total spectroscopic data acquisition time was less than 13 min. The nominal voxel size was 0.67 × 0.67 × 1.0 cm^3 (~0.45-cm^3 resolution). After zero filling to a matrix size of 32 × 32, the volume of a voxel relevant for postprocessing was 0.25 cm^3.

The user-independent spectral fit program LCModel (Linear Combination of Model, version 6.1-4A) (s-provencher.com) (*14*) was used for the quantitative evaluation of ^{1}H MRSI data. The spectra were analyzed on a workstation (IBM Lenovo) as a linear combination of a set of reference basis spectra for PRESS and a TE of 135 ms. For calibration of the LCModel program and for determination of the metabolite concentrations for Cho, Cr, and tNAA, we used the phantom replacement technique (*9,15*). Voxel positions in the lesions and in contralateral apparently normal brain tissue were selected. Spectral fits were performed in an analysis window of 1.0–3.85 ppm. Spectra with a signal-to-noise ratio of less than 2 and a full width at half maximum of greater than 0.075 ppm were not included. All molar metabolite concentrations were corrected for relaxation time effects with T1 and T2 times from the literature (*16*).

Radiosynthesis of ^{18}F-FET and ^{18}F-FET PET Data Acquisition

Starting from ^{18}F-fluoride that was produced by the ^{18}O(p,n)^{18}F reaction on ^{18}O-enriched water (95%) with an 11-MeV proton beam generated by an RDS 111 cyclotron (PET Net GmbH), ^{18}F-FET was synthesized via ^{18}F-fluoroalkylation of the disodium salt of L-tyrosine by ^{18}F-fluoroethyltosylate, in accordance with the procedure of Wester et al. (*17*). The 2-step procedure was performed by use of an automated synthesis module consisting of a Simatic S7-200 device (Siemens) and ProTool/Pro software (Siemens). ^{18}F-FET was obtained as an intravenously injectable phosphate-buffered saline solution (pH 5.5) (490 ± 320 [mean ± SD] MBq/mL) containing tyrosine at 9–57 μg/mL. The non–decay-corrected radiochemical yield was about 18% at a molar radioactivity of greater than 150 GBq/μmol, and the radiochemical purity was at least 97%.

^{18}F-FET PET scans from the brain were performed 10 min after the intravenous injection of ^{18}F-FET at 7 MBq/kg of body weight. A partial-ring PET scanner (ECAT EMERGE; Siemens) equipped with lutetium oxyorthosilicate detectors was used. The technical performance of this machine was described recently (*18*). The measured attenuation correction scan time of transmission was 7 min. Emission data were acquired over 24 min (4 frames over 6 min). The ECAT EMERGE scanner allows data acquisition in the 3D mode only. Emission data corrected for randoms, dead time, and attenuation were reconstructed with an iterative reconstruction algorithm (ordered-subset expectation maximization; 4 iterations, 8 subsets). The number of projections and views was 192, the matrix size was 128 × 128 in plane, the voxel side length was 0.515 cm, the reconstructed image resolution was approximately 6.5 mm, the zoom was 2.57, and the slice thickness was 3.4 mm.

Coregistration of ^{1}H MRSI and ^{18}F-FET PET Data

For the coregistration of ^{18}F-FET PET and ^{1}H MRSI data, both datasets were previously coregistered with an anatomic 3D MRI dataset (MPRAGE). For this purpose, the ^{1}H MRSI data were evaluated as metabolic maps of Cho and tNAA by use of the freely available reconstruction program csx (version for Linux; Kennedy Krieger Institute). The peak areas for Cho and tNAA were calculated by integration over frequency ranges of 3.34–3.14 and 2.22–1.82 ppm, respectively. Smooth linear interpolation to a matrix size of 256 × 256 resulted in metabolic maps. Cho and tNAA images were used to calculate a map of Cho/tNAA ratios. Segmentation of the tumor on the basis of the metabolic changes related to the lesion on the Cho/tNAA ratio map was performed by a method described previously (*19*). A Cho/tNAA ratio map is particularly suited for delineation of brain tumors because it uses both the increase in Cho levels and the decrease in tNAA levels in lesions, resulting in enhanced contrast. Furthermore, in normal brain parenchyma, Cho/tNAA ratios show a gaussian distribution and are quite constant (*19*).

A so-called MRI/MRSI hybrid dataset, which consisted of anatomic MR images (T1-weighted SE sequence) and metabolic maps from the ^{1}H MRSI data, was generated. Both the MRI/MRSI hybrid dataset and the ^{18}F-FET PET data were transferred to a workstation (IBM Lenovo) for coregistration by use of the graphic image analysis tool VINCI (Volume Imaging in Neurologic Research; Max-Planck-Institute for Neurologic Research) (*20*). Coregistration of the ^{18}F-FET PET data (Fig. 1A) and the ^{1}H MRSI data (Fig. 1B) with the 3D MPRAGE dataset was achieved by use of a rigid registration algorithm. The fused dataset consisted of anatomic MR images, PET images, and metabolic maps from ^{1}H MRSI and allowed for the direct correlation of ^{18}F-FET uptake with metabolic concentrations for Cho, Cr, and tNAA and Cho/tNAA ratios (Fig. 1C).

Regions of interest (ROIs) were manually defined on PET images to segment lesions into 4 different areas according to ^{18}F-FET uptake and in the contralateral normal brain (CNB). These areas were defined as follows: maximum ^{18}F-FET uptake, which was defined as the area with the maximum uptake of ^{18}F-FET in the lesion under study; strong ^{18}F-FET uptake, which was defined as the area with ^{18}F-FET uptake of less than the maximum but ≥75% of the maximum; moderate ^{18}F-FET uptake, which was defined as the area with ^{18}F-FET uptake of less than 75% but ≥50% of the maximum; and low ^{18}F-FET uptake, which was defined as the area with ^{18}F-FET uptake of less than 50% but ≥25% of the maximum (Fig. 2A). No defined area included any

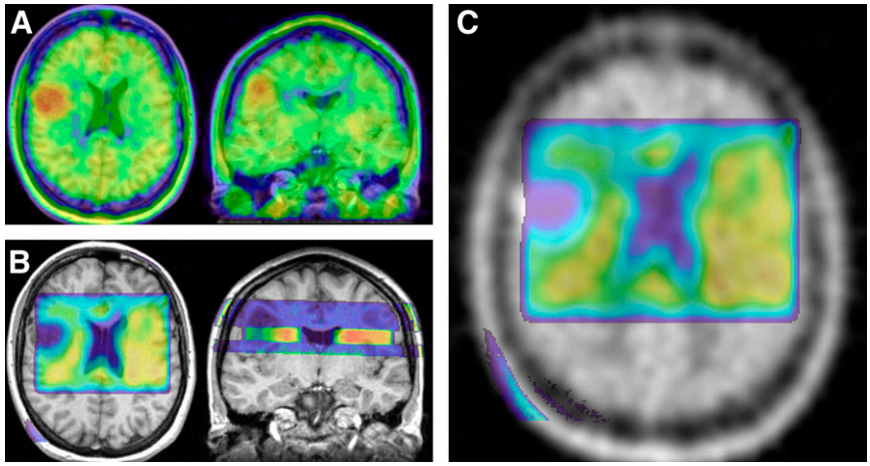

FIGURE 1. Procedure for coregistering ^{18}F-FET PET and ^{1}H MRSI data for patient 3. (A) Axial and coronal images of fused ^{18}F-FET PET and anatomic MRI dataset, obtained by coregistration of color-coded PET dataset (color code: red = maximum ^{18}F-FET uptake and blue = minimum ^{18}F-FET uptake) with 3D MPRAGE dataset. (B) Axial and sagittal images of fused ^{1}H MRSI data (evaluated as tNAA metabolic map) and anatomic MRI data, obtained by coregistration of color-coded MRI/MRSI hybrid dataset (color code: red = maximum tNAA concentration and blue = minimum tNAA concentration) with 3D MPRAGE dataset. (Sagittal image shows MRI/MRSI hybrid dataset consisting of anatomic information in blue above and below tNAA metabolic map.) (C) Axial image of coregistered ^{18}F-FET PET dataset (gray scale) and tNAA metabolic map (color coded) calculated from ^{1}H MRSI dataset.

part of another defined area. The area with strong ^{18}F-FET uptake, for example, did not include the area with maximum ^{18}F-FET uptake. The area with maximum ^{18}F-FET uptake was selected as a target for the stereotactic biopsy. A minimum volume of 1 cm^3 was required as a target volume for the stereotactic procedure. In addition, this approach minimized partial-volume effects between ^{18}F-FET PET and ^{1}H MRSI, which were acquired at different spatial resolutions. The mean ^{18}F-FET uptake values were calculated for these ROIs in the tumor and for the ROI in the CNB and used for the calculation of tumor-to-brain ratios (TBR) of ^{18}F-FET uptake. The ROI in the CNB was equal in size to the sum of all 4 tumor ROIs.

Additionally, the ROIs that were defined on the PET dataset were copied to the coregistered ^{1}H MRSI dataset (Fig. 2B) and used for calculation of the mean metabolite concentrations for Cho, Cr, and tNAA and Cho/tNAA ratios in the corresponding areas. The congruence of the areas of increased ^{18}F-FET uptake and the areas of increased Cho/tNAA ratios in the lesions was estimated on the coregistered PET and ^{1}H MRSI datasets. The same estimation of congruence was performed for the areas of maximum ^{18}F-FET uptake and the areas of maximum changes in Cho/tNAA ratios by use of a 3-stage scale system: scale 2 for more than 50% overlap of the areas with maximum pathologic changes, scale 1 for less than 50% overlap, and scale 0 for no overlap (Fig. 3).

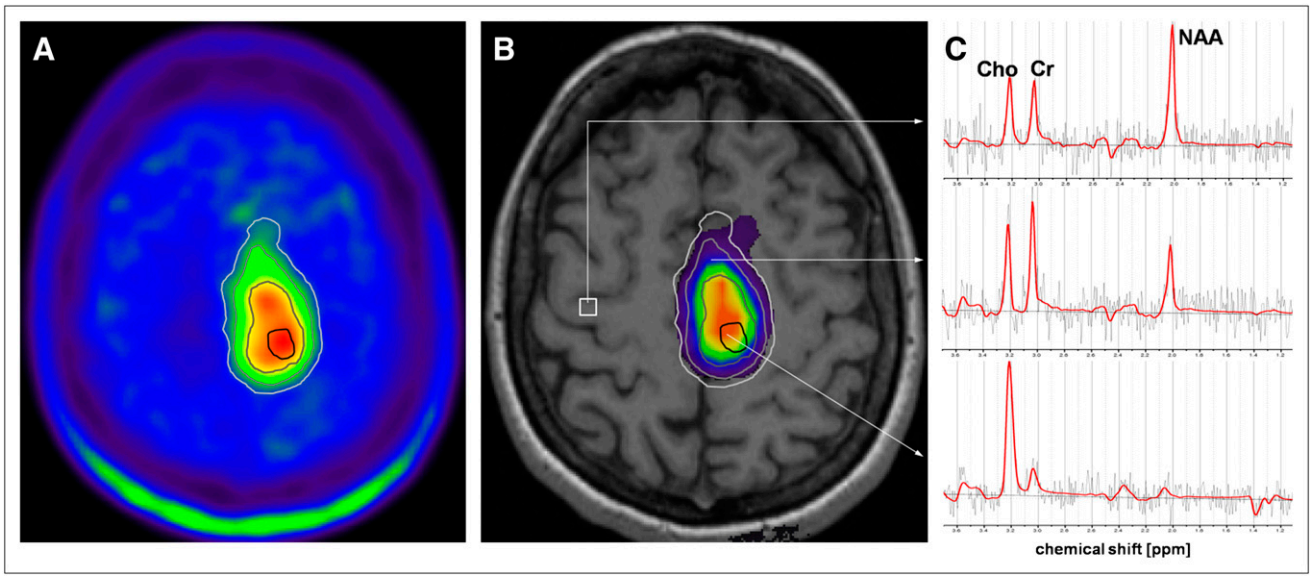

FIGURE 2. Segmentation of areas in lesion with different levels of ^{18}F-FET uptake and copy of ROIs to ^{1}H MRSI data for patient 5. (A) Axial PET image with manually defined ROIs for segmentation of areas with maximum ^{18}F-FET uptake (black line), strong ^{18}F-FET uptake (dark gray line), moderate ^{18}F-FET uptake (gray line), and low ^{18}F-FET uptake (light gray line). (B) Corresponding Cho/tNAA ratio map and ROIs overlaid on anatomic MR image. (C) LCModel fits (red line) of representative spectra. Upper spectrum is from voxel position in CNB (white square on B), middle spectrum is from voxel in area with moderate ^{18}F-FET uptake, and lower spectrum is from voxel in area with maximum ^{18}F-FET uptake.

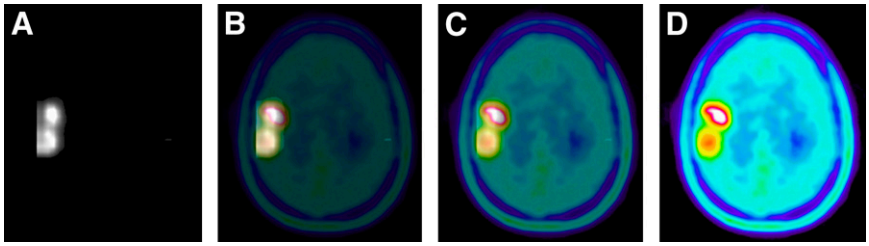

FIGURE 3. Series of images with variable opacities illustrating fusion of segmented Cho/tNAA ratio maps and ^{18}F-FET PET images from patient 3. (A) Segmented Cho/tNAA ratio map with 100% opacity. (B and C) Fusion of segmented Cho/tNAA ratio map (with 75% opacity [B] and 25% opacity [C]) and ^{18}F-FET PET images (with 25% opacity [B] and 75% opacity [C]). (D) ^{18}F-FET PET image with 100% opacity.

Statistical Analysis

Data were analyzed by use of SPSS statistical software (version 14.0; SPSS). Spearman ρ correlation coefficients were calculated by linear regression analyses of correlations between TBR of ^{18}F-FET uptake and metabolite data (Cho, Cr, and tNAA concentrations and Cho/tNAA ratios). Comparisons of TBR of ^{18}F-FET uptake and metabolite data in the 4 tumor areas and in the CNB between groups (patients with gliomas of WHO grade II, those with gliomas of WHO grade III, and those with GBM of WHO grade IV) were performed by use of the Mann–Whitney *U* test. Probability values of less than 0.05 were considered significant. A correction for multiple comparisons was not applied.

RESULTS

Coregistration of ^{1}H MRSI and ^{18}F-FET PET was successful for data from all 15 patients. Figure 2C shows representative spectra from a voxel position in the CNB (upper spectrum), from a voxel in the area with moderate ^{18}F-FET uptake (middle spectrum), and from a voxel in the area with maximum ^{18}F-FET uptake (lower spectrum). For all 15 patients, the overlap of ^{18}F-FET uptake and Cho/tNAA ratio data was more than 75%. The results of evaluating congruence for the areas of maximum ^{18}F-FET uptake and maximum changes in Cho/tNAA ratios are shown in Table 1. Congruence of these "maximum" areas was found for all 15 patients. For 11 patients (73%), there was an overlap of more than 50% (Figs. 2 and 3), and for 4 patients (27%), there was an overlap of less than 50%. For the latter patients, the distances between the ^{18}F-FET uptake maxima and the Cho/tNAA ratio maxima were 8.5–21 mm (mean ± SD, 13.5 ± 5.3 mm).

The results of the linear regression analyses of the correlations of ^{18}F-FET uptake and ^{1}H MRSI metabolite changes are shown in Table 2. The strongest correlations with ^{18}F-FET uptake (TBR in tumor areas with maximum, strong, and moderate ^{18}F-FET uptake) were found for Cho/tNAA ratios in areas with maximum and strong ^{18}F-FET uptake and for tNAA in areas with maximum ^{18}F-FET uptake. However, no significant correlation was registered for these two ^{1}H MRSI parameters in the area with low ^{18}F-FET uptake. Cho showed no significant correlation with ^{18}F-FET uptake. Regression analysis of the TBR of ^{18}F-FET uptake versus Cr revealed a significant correlation in the area with low ^{18}F-FET uptake. In the CNB, no significant correlation was found for ^{1}H MRSI metabolite changes and ^{18}F-FET uptake. Figure 4 shows examples of scatter plots for significant correlations of Cho/tNAA ratios and tNAA in the area with maximum ^{18}F-FET uptake

TABLE 2
Correlations of ^{18}F-FET Uptake and ^{1}H MRSI Metabolite Data

Area of ^{18}F-FET uptake	*R* for:			
	Cho	Cr	tNAA	Cho/tNAA
Maximum	0.475	−0.064	−0.557*	0.945†
Strong	0.492	0.464	−0.404	0.811†
Moderate	0.164	0.471	−0.482	0.531*
Low	0.072	0.626*	−0.089	0.095
CNB	−0.134	−0.290	0.384	−0.329
All tumor areas‡	0.501†	−0.022	−0.880†	0.891†
Tumors of following WHO grade§ (no. of subjects):				
II (4)	0.535*	−0.126	−0.871†	0.849†
III (6)	0.406*	0.007	−0.845†	0.851†
IV (5)	0.705†	0.036	−0.913†	0.947†

*$P < 0.05$.
†$P < 0.001$.
‡Correlations for combination of all 4 areas in lesions (maximum to low ^{18}F-FET uptake).
§Correlations for all tumor areas in subgroups of patients with WHO grade II, III, and IV gliomas. Patient with gliomatosis cerebri was included in group of patients with glioma of WHO grade III.

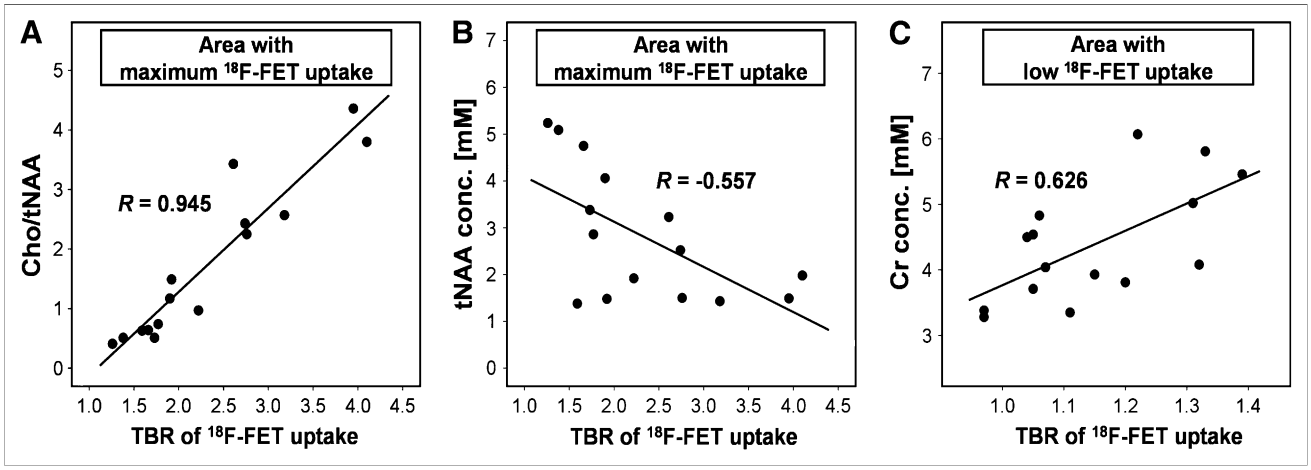

FIGURE 4. Scatter plots of correlations between metabolite data determined with ^{1}H MRSI and TBR of ^{18}F-FET uptake for all 15 patients with gliomas. Overlaid are Spearman ρ correlation coefficients from linear regression analyses. (A and B) Significant correlations between Cho/tNAA ratio and TBR of ^{18}F-FET uptake ($P < 0.001$) (A) and between tNAA concentration and TBR of ^{18}F-FET uptake ($P = 0.031$) (B) in area with maximum ^{18}F-FET uptake. (C) Significant correlation between Cr concentration (conc.) and TBR of ^{18}F-FET uptake in area with low ^{18}F-FET uptake ($P = 0.013$).

(Figs. 4A and 4B) and Cr in the area with low ^{18}F-FET uptake (Fig. 4C).

For the combination of all 4 tumor areas (i.e., maximum to low ^{18}F-FET uptake), regression analyses revealed significant correlations for Cho, tNAA, and Cho/tNAA ratios and the TBR of ^{18}F-FET uptake (Table 2). Similar results were found when the WHO grades of the lesions were considered (Table 2).

A Mann–Whitney *U* test for the comparison of ^{18}F-FET uptake in subgroups of patients with gliomas of different WHO grades revealed significant differences ($P = 0.032$) in maximum ^{18}F-FET uptake between gliomas of WHO grade II and GBM of WHO grade IV. For Cho, Cr, and tNAA concentrations and Cho/tNAA ratios, a Mann–Whitney *U* test revealed significant differences ($P = 0.016$) in tNAA concentrations in areas with maximum, strong, and moderate ^{18}F-FET uptake between WHO grade II and IV gliomas.

Figure 5 shows box plots of the TBR of ^{18}F-FET uptake, tNAA concentrations, and Cho/tNAA ratios in the area with maximum ^{18}F-FET uptake for the 3 subgroups of patients.

DISCUSSION

Several studies have demonstrated the benefit of ^{18}F-FET PET for the management of gliomas in terms of differential diagnosis and grading (*21–23*), in the prognosis of patient outcomes (*24*), in therapy monitoring (*25*), and in the de-

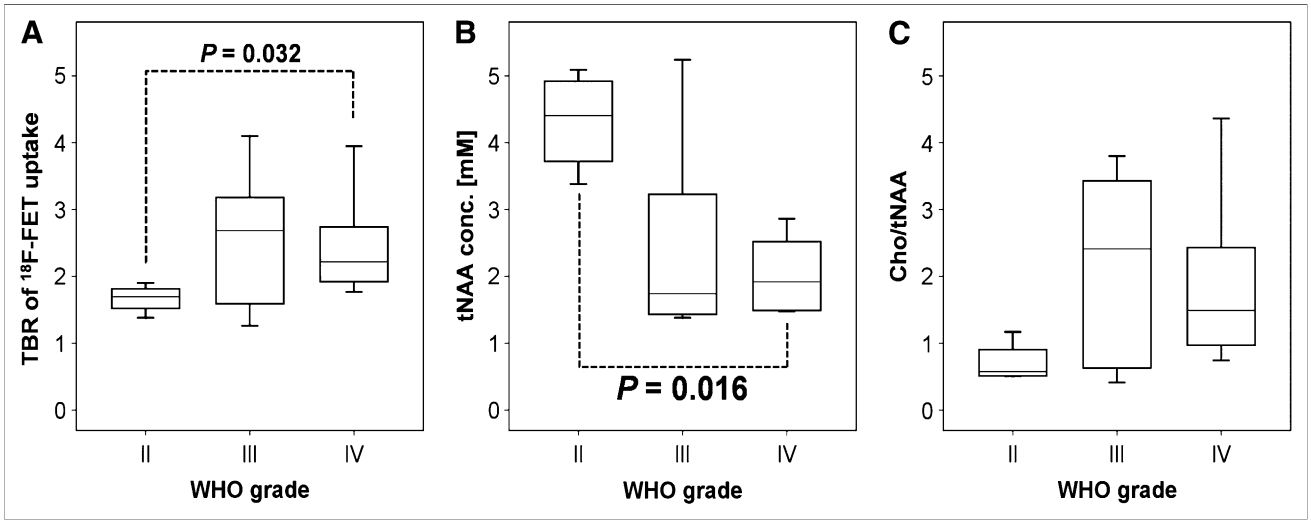

FIGURE 5. Box plots of TBR of ^{18}F-FET uptake (A), tNAA concentration (conc.) (B), and Cho/tNAA ratio (C) in area with maximum ^{18}F-FET uptake for groups of patients with gliomas of WHO grades II, III, and IV. Significant differences between subgroups are marked with dotted lines, and *P* values are overlaid.

tection and diagnosis of tumor recurrence (*26–28*). Pauleit et al. (*21*) demonstrated an improvement in diagnostic accuracy when a combination of MRI and ^{18}F-FET PET was used to delineate tumor borders. They found a sensitivity of 96% and a specificity of 53% for the detection of tumor tissue with MRI alone and a sensitivity of 93% and a specificity of 94% with the combination of MRI and ^{18}F-FET PET.

However, the mechanisms of uptake and retention of ^{18}F-FET in different parts of lesions are not yet fully clarified. Early in vitro and in vivo studies have shown that ^{18}F-FET is not incorporated into proteins but that uptake into tumor cells occurs via specific amino acid carrier systems (*17,29*). A comparative study by Langen et al. (*30*) suggested that ^{18}F-FET transport in F98 rat gliomas occurs via both Na^+-independent system L and the $^+$-dependent system $B^{0,+}$. However, clinical studies of different tumor types have indicated that the situation is more complex (*7*). For brain tumors specifically, the influence of the disruption of the blood–brain barrier has been discussed (*22,25,31,32*). Spaeth et al. (*31,32*) concluded from their results of a ^{18}F-FET PET study in F98 rat gliomas that increased ^{18}F-FET uptake may be facilitated by the tumor cells themselves, whereas active transport across the blood–brain barrier is probably not a rate-limiting factor. They further concluded that disruption of the blood–brain barrier may result in the leakage of ^{18}F-FET into the interstitial space (*31,32*).

Recent studies by Salber et al. investigated the uptake of ^{18}F-FET in comparison with the uptake of ^{3}H-methionine and ^{3}H-deoxyglucose in brain abscesses (*33*) and ^{3}H-methionine in focal cortical ischemia in rat models (*34*). They found discrepancies between the rates of uptake of the tracers in these nonneoplastic lesions, indicating that nonspecifically increased ^{18}F-FET uptake may be related to reactive astrocytosis.

A few studies involved combined metabolic measurements for gliomas with ^{18}F-FDG PET and magnetic resonance spectroscopy (MRS). Most of these studies reported correlations between glucose metabolism and ^{1}H MRSI–derived variables (*35–39*). Kwee et al. (*40*) performed ^{18}F-fluorocholine PET and ^{1}H MRSI for 2 patients with intracranial lesions; 1 had a demyelinating process, and 1 had GBM. They demonstrated significant correlations between the mean and maximum standardized uptake values of the radiopharmaceutical and the regional Cho/Cr ratio for the patient with GBM but not for the patient with the demyelinating process.

As yet, only one other multimodal metabolic imaging study combining ^{18}F-FET PET and ^{1}H MRSI for gliomas has been published (*41*). Floeth et al. (*41*) determined the predictive value of ^{18}F-FET PET and single-voxel ^{1}H MRSI for the differential diagnosis of benign and malignant cerebral lesions with a lesion-to-brain ratio of ^{18}F-FET uptake of greater than 1.6 and an NAA/Cho ratio of less than 0.7 as tumor indicators. Compared with conventional MRI, they reported an increase in diagnostic accuracy for the combination of MRI with ^{18}F-FET PET and ^{1}H MRSI for this purpose. Plotkin et al. (*42*) performed SPECT with ^{123}I-iodomethyltyrosine and single-voxel MRS for differentiation between residual tumor or recurrence and treatment-related changes in pretreated patients with gliomas (*42*). They found that ^{123}I-iodomethyltyrosine had higher sensitivity, specificity, and accuracy than single-voxel MRS for distinguishing the changes.

In contrast, our purpose was to correlate the spatial heterogeneity of ^{18}F-FET PET and multivoxel ^{1}H MRSI for gliomas. This spatial heterogeneity most likely reflects different extents of tumor infiltration. We performed multimodal metabolic imaging of cerebral gliomas to correlate differences in ^{18}F-FET uptake in the lesion with metabolite concentrations for Cho, Cr, and tNAA and Cho/tNAA ratios. Our purpose was to obtain multimodal metabolic information from tumor areas with variable degrees of pathology.

We found congruence between elevated ^{18}F-FET uptake and increases in Cho/NAA ratios for the delineation of the whole tumor as well as for the detection of maximum pathologic changes. Although both modalities detected different metabolic activities in the lesions, they provided comparable results in delineating pathologic changes most likely reflecting tumor infiltration.

In areas with maximum, strong, and moderate ^{18}F-FET uptake, a significant correlation of that variable with the Cho/tNAA ratio, that is, the ratio of membrane turnover to neuronal loss, was found. The concentration of tNAA, that is, the absolute extent of neuronal loss, showed a significant correlation only in areas with maximum ^{18}F-FET uptake. In recent studies, we were able to demonstrate that a strong correlation exists between the extent of tumor cell infiltration and tNAA and Cho/tNAA ratio (*9*). It is legitimate to conclude that the same correlation exists between ^{18}F-FET uptake and tumor cell infiltration. These data corroborate the findings of earlier studies, providing evidence for the usefulness of ^{18}F-FET PET in determining tumor extent (*21,22,27,28*).

An interesting and unexpected result was the correlation of the Cr concentration, a marker of energy metabolism, with amino acid accumulation in areas with low ^{18}F-FET uptake. This correlation may have been associated with the mechanisms of tumor infiltration into normal brain tissue or the immune response of brain parenchyma. This hitherto unreported observation deserves further investigation.

We found significant differences in maximum ^{18}F-FET uptake and the tNAA concentration between WHO grade II and IV gliomas but not for between these 2 tumor grades and WHO grade III. Because of the small number of patients in the subgroups of patients with different WHO grades (4 patients had gliomas of WHO grade II), we decided not to compare low-grade gliomas (4 patients) and high-grade gliomas (11 patients). However, our findings for maximum ^{18}F-FET uptake are in good agreement with the results of previous studies investigating the kinetics of ^{18}F-FET uptake. In our study, PET scans were performed in an early phase, starting 10 min after injection. Significant

differences in ^{18}F-FET uptake between low- and high-grade gliomas were documented for untreated gliomas in the first 10 min after injection (*22*) as well as for recurrent gliomas at 5–20 min after injection (*26*). An ^{18}F-FET PET data acquisition starting more than 20 min after injection seems to result in ^{18}F-FET uptake values that are not significantly different in low- and high-grade gliomas (*21,22,26,27*).

Our data may be considered preliminary in view of the comparatively small number of subjects studied. A further limitation is the fact that we performed the ^{1}H MRSI experiment as a 2-dimensional experiment. To cover the entire or at least the bulk of the tumor volume, it will be necessary to use a 3D ^{1}H MRSI sequence with a spatial resolution comparable to those of PET scans. The latter has the drawbacks of longer acquisition times and a decline in the signal-to-noise ratio. The application of so-called parallel imaging techniques (e.g., sensitivity-encoded spectroscopic imaging) (*43*) at higher magnetic field strengths (3 T or more) (*44*) would be a strategy for overcoming this problem. However, ^{1}H MRSI is very sensitive to susceptibility artifacts, a property that excludes the use of this method in patients with tumors in subcranial, frontobasal, or temporal locations or in patients after surgery. Unfortunately, these problems are more evident at higher magnetic field strengths. On the other hand, in theory, ^{1}H MRSI can be performed with any modern MR scanner, provided that a license exists, whereas the availability of ^{18}F-FET PET is still limited.

CONCLUSION

In this study, we demonstrated a significant correlation between amino acid uptake assessed with ^{18}F-FET PET and various parameters derived from ^{1}H MRSI data for patients with gliomas. In the tumor center, the increase in ^{18}F-FET transport correlates with the extent of neuronal loss (tNAA) and correlates partially with the extent of the increase in membrane proliferation (Cho). The correlation of the marker for energy metabolism (Cr) with ^{18}F-FET uptake in the tumor border needs to be investigated in further studies. This is the first study correlating the spatial heterogeneity of changes in amino acid transport assessed with ^{18}F-FET PET and parameters derived from ^{1}H MRSI. Both methods provided complementary information in the study of glioma metabolism that may be useful in planning and targeting surgery and radiochemotherapy.

ACKNOWLEDGMENTS

The authors thank Wilhelm Hamkens and Dr. Willi Kalender (PET Net GmbH, Erlangen, Germany) for expert technical support and excellent collaboration.

REFERENCES

1. Kaim AH, Weber B, Kurrer MO, Gottschalk J, Von Schulthess GK, Buck A. Autoradiographic quantification of ^{18}F-FDG uptake in experimental soft-tissue abscesses in rats. *Radiology.* 2002;223:446–451.
2. Kubota R, Yamada S, Kubota K, Ishiwata K, Tamahashi N, Ido T. Intratumoral distribution of fluorine-18-fluorodeoxyglucose in vivo: high accumulation in macrophages and granulation tissues studied by microautoradiography. *J Nucl Med.* 1992;33:1972–1980.
3. Deichen JT, Prante O, Gack M, Schmiedehausen K, Kuwert T. Uptake of [^{18}F]fluorodeoxyglucose in human monocyte-macrophages in vitro. *Eur J Nucl Med Mol Imaging.* 2003;30:267–273.
4. Kaim AH, Weber B, Kurrer MO, et al. ^{18}F-FDG and ^{18}F-FET uptake in experimental soft tissue infection. *Eur J Nucl Med Mol Imaging.* 2002;29: 648–654.
5. Rau FC, Weber WA, Wester HJ, et al. O-(2-[^{18}F]Fluoroethyl)-L-tyrosine (FET): a tracer for differentiation of tumour from inflammation in murine lymph nodes. *Eur J Nucl Med Mol Imaging.* 2002;29:1039–1046.
6. Prante O, Blaser D, Maschauer S, Kuwert T. In vitro characterization of the thyroidal uptake of O-(2-[^{18}F]fluoroethyl)-L-tyrosine. *Nucl Med Biol.* 2007;34: 305–314.
7. Langen KJ, Hamacher K, Weckesser M, et al. O-(2-[^{18}F]Fluoroethyl)-L-tyrosine: uptake mechanisms and clinical applications. *Nucl Med Biol.* 2006;33: 287–294.
8. Majos C, Alonso J, Aguilera C, et al. Adult primitive neuroectodermal tumor: proton MR spectroscopic findings with possible application for differential diagnosis. *Radiology.* 2002;225:556–566.
9. Stadlbauer A, Gruber S, Nimsky C, et al. Preoperative grading of gliomas by using metabolite quantification with high-spatial-resolution proton MR spectroscopic imaging. *Radiology.* 2006;238:958–969.
10. Sabatier J, Gilard V, Malet-Martino M, et al. Characterization of choline compounds with in vitro ^{1}H magnetic resonance spectroscopy for the discrimination of primary brain tumors. *Invest Radiol.* 1999;34:230–235.
11. Moffett JR, Ross B, Arun P, Madhavarao CN, Namboodiri AM. N-Acetylaspartate in the CNS: from neurodiagnostics to neurobiology. *Prog Neurobiol.* 2007;81:89–131.
12. Kemp GJ. Non-invasive methods for studying brain energy metabolism: what they show and what it means. *Dev Neurosci.* 2000;22:418–428.
13. Stadlbauer A, Moser E, Gruber S, Nimsky C, Fahlbusch R, Ganslandt O. Integration of biochemical images of a tumor into frameless stereotaxy achieved using a magnetic resonance imaging/magnetic resonance spectroscopy hybrid data set. *J Neurosurg.* 2004;101:287–294.
14. Provencher SW. Estimation of metabolite concentrations from localized in vivo proton NMR spectra. *Magn Reson Med.* 1993;30:672–679.
15. McLean MA, Woermann FG, Barker GJ, Duncan JS. Quantitative analysis of short echo time ^{1}H-MRSI of cerebral gray and white matter. *Magn Reson Med.* 2000;44:401–411.
16. Isobe T, Matsumura A, Anno I, et al. Quantification of cerebral metabolites in glioma patients with proton MR spectroscopy using T2 relaxation time correction. *Magn Reson Imaging.* 2002;20:343–349.
17. Wester HJ, Herz M, Weber W, et al. Synthesis and radiopharmacology of *O*-(2-^{18}F-fluoroethyl)-L-tyrosine for tumor imaging. *J Nucl Med.* 1999;40: 205–212.
18. Herzog H, Tellmann L, Hocke C, Pietrzyk U, Casey ME, Kuwert T. NEMA NU2-2001 guided performance evaluation of four Siemens ECAT PET-Scanners. *IEEE Trans Nucl Sci.* 2004;51:2662–2669.
19. Stadlbauer A, Moser E, Gruber S, et al. Improved delineation of brain tumors: an automated method for segmentation based on pathologic changes of ^{1}H-MRSI metabolites in gliomas. *Neuroimage.* 2004;23:454–461.
20. Cizek J, Herholz K, Vollmar S, Schrader R, Klein J, Heiss WD. Fast and robust registration of PET and MR images of human brain. *Neuroimage.* 2004;22: 434–442.
21. Pauleit D, Floeth F, Hamacher K, et al. O-(2-[^{18}F]Fluoroethyl)-L-tyrosine PET combined with MRI improves the diagnostic assessment of cerebral gliomas. *Brain.* 2005;128:678–687.
22. Weckesser M, Langen KJ, Rickert CH, et al. O-(2-[^{18}F]Fluorethyl)-L-tyrosine PET in the clinical evaluation of primary brain tumours. *Eur J Nucl Med Mol Imaging.* 2005;32:422–429.
23. Floeth FW, Pauleit D, Sabel M, et al. ^{18}F-FET PET differentiation of ring-enhancing brain lesions. *J Nucl Med.* 2006;47:776–782.
24. Floeth FW, Pauleit D, Sabel M, et al. Prognostic value of *O*-(2-^{18}F-fluoroethyl)-L-tyrosine PET and MRI in low-grade glioma. *J Nucl Med.* 2007;48:519–527.
25. Pöpperl G, Goldbrunner R, Gildehaus FJ, et al. O-(2-[^{18}F]Fluoroethyl)-L-tyrosine PET for monitoring the effects of convection-enhanced delivery of paclitaxel in patients with recurrent glioblastoma. *Eur J Nucl Med Mol Imaging.* 2005;32:1018–1025.
26. Pöpperl G, Kreth FW, Herms J, et al. Analysis of ^{18}F-FET PET for grading of recurrent gliomas: is evaluation of uptake kinetics superior to standard methods? *J Nucl Med.* 2006;47:393–403.

27. Pöpperl G, Gotz C, Rachinger W, Gildehaus FJ, Tonn JC, Tatsch K. Value of O-(2-[^{18}F]fluoroethyl)-L-tyrosine PET for the diagnosis of recurrent glioma. *Eur J Nucl Med Mol Imaging.* 2004;31:1464–1470.
28. Rachinger W, Goetz C, Pöpperl G, et al. Positron emission tomography with O-(2-[^{18}F]fluoroethyl)-l-tyrosine versus magnetic resonance imaging in the diagnosis of recurrent gliomas. *Neurosurgery.* 2005;57:505–511.
29. Heiss P, Mayer S, Herz M, Wester HJ, Schwaiger M, Senekowitsch-Schmidtke R. Investigation of transport mechanism and uptake kinetics of *O*-(2-^{18}F-fluoroethyl)-L-tyrosine in vitro and in vivo. *J Nucl Med.* 1999;40:1367–1373.
30. Langen KJ, Jarosch M, Muhlensiepen H, et al. Comparison of fluorotyrosines and methionine uptake in F98 rat gliomas. *Nucl Med Biol.* 2003;30:501–508.
31. Spaeth N, Wyss MT, Pahnke J, et al. Uptake of ^{18}F-fluorocholine, ^{18}F-fluoro-ethyl-L: -tyrosine and ^{18}F-fluoro-2-deoxyglucose in F98 gliomas in the rat. *Eur J Nucl Med Mol Imaging.* 2006;33:673–682.
32. Spaeth N, Wyss MT, Weber B, et al. Uptake of ^{18}F-fluorocholine, ^{18}F-fluoroethyl-L-tyrosine, and ^{18}F-FDG in acute cerebral radiation injury in the rat: implications for separation of radiation necrosis from tumor recurrence. *J Nucl Med.* 2004;45:1931–1938.
33. Salber D, Stoffels G, Pauleit D, et al. Differential uptake of *O*-(2-^{18}F-fluoroethyl)-L-tyrosine, L-^{3}H-methionine, and ^{3}H-deoxyglucose in brain abscesses. *J Nucl Med.* 2007;48:2056–2062.
34. Salber D, Stoffels G, Pauleit D, et al. Differential uptake of [^{18}F]FET and [^{3}H]l-methionine in focal cortical ischemia. *Nucl Med Biol.* 2006;33:1029–1035.
35. Lichy MP, Bachert P, Henze M, Lichy CM, Debus J, Schlemmer HP. Monitoring individual response to brain-tumour chemotherapy: proton MR spectroscopy in a patient with recurrent glioma after stereotactic radiotherapy. *Neuroradiology.* 2004;46:126–129.
36. Lichy MP, Henze M, Plathow C, Bachert P, Kauczor HU, Schlemmer HP. Metabolic imaging to follow stereotactic radiation of gliomas: the role of 1H MR spectroscopy in comparison to FDG-PET and IMT-SPECT [in German]. *Rofo.* 2004;176:1114–1121.
37. Schlemmer HP, Bachert P, Henze M, et al. Differentiation of radiation necrosis from tumor progression using proton magnetic resonance spectroscopy. *Neuroradiology.* 2002;44:216–222.
38. Alger JR, Frank JA, Bizzi A, et al. Metabolism of human gliomas: assessment with H-1 MR spectroscopy and F-18 fluorodeoxyglucose PET. *Radiology.* 1990;177:633–641.
39. Luyten PR, Marien AJ, Heindel W, et al. Metabolic imaging of patients with intracranial tumors: H-1 MR spectroscopic imaging and PET. *Radiology.* 1990; 176:791–799.
40. Kwee SA, Coel MN, Lim J, Ko JP. Combined use of F-18 fluorocholine positron emission tomography and magnetic resonance spectroscopy for brain tumor evaluation. *J Neuroimaging.* 2004;14:285–289.
41. Floeth FW, Pauleit D, Wittsack HJ, et al. Multimodal metabolic imaging of cerebral gliomas: positron emission tomography with [^{18}F]fluoroethyl-L-tyrosine and magnetic resonance spectroscopy. *J Neurosurg.* 2005;102:318–327.
42. Plotkin M, Eisenacher J, Bruhn H, et al. ^{123}I-IMT SPECT and ^{1}H MR-spectroscopy at 3.0 T in the differential diagnosis of recurrent or residual gliomas: a comparative study. *J Neurooncol.* 2004;70:49–58.
43. Dydak U, Weiger M, Pruessmann KP, Meier D, Boesiger P. Sensitivity-encoded spectroscopic imaging. *Magn Reson Med.* 2001;46:713–722.
44. Gruber S, Mlynarik V, Moser E. High-resolution 3D proton spectroscopic imaging of the human brain at 3 T: SNR issues and application for anatomy-matched voxel sizes. *Magn Reson Med.* 2003;49:299–306.